metals

MDPI

Article

Biofunctionalization of Porous Ti Substrates Coated with Ag Nanoparticles for Potential Antibacterial Behavior

Juliana Gaviria [1], Ana Alcudia [2], Belén Begines [2,*], Ana María Beltrán [3], José Antonio Rodríguez-Ortiz [3], Paloma Trueba [3], Junes Villarraga [1] and Yadir Torres [3]

[1] Grupo de Biomateriales Avanzados y Medicina Regenerativa, BAMR, Bioengineering Program, University of Antioquia, Calle 67, 53-108, Medellín 50011, Colombia; julitorre3@hotmail.com (J.G.); junesabdul@gmail.com (J.V.)
[2] Departamento de Química Orgánica y Farmacéutica, Facultad de Farmacia, Universidad de Sevilla, 41012 Seville, Spain; aalcudia@us.es
[3] Departamento de Ingeniería y Ciencia de los Materiales y del Transporte, Escuela Politécnica Superior, Universidad de Sevilla, 41011 Seville, Spain; abeltran3@us.es (A.M.B.); jarortiz@us.es (J.A.R.-O.); ptrueba@us.es (P.T.); ytorres@us.es (Y.T.)
* Correspondence: bbegines@us.es

Abstract: Ti prosthesis have shown better biological compatibility, mechanical performance, and resistance to corrosion in cases of bone replacements. Nevertheless, fully dense Ti in connection with bone-host tissues show stress-shielding phenomenon that, together with the development of frequent undesirable microbial infections, may lead to implant failures. To overcome these issues, the present study aimed at the development of a novel combination of a chemically functionalized porous Ti substrate with a potentially therapeutic AgNPs coating. Fully dense and porous Ti substrates (30 and 60 vol.%, 100–200 and 355–500 µm, as spacer particles) were studied. Ti surface was treated with acid or basic medium followed by silanization and deposition of AgNPs by "submerged" and "in situ" methods. In general, for similar porosity, mechanical resistance decreased as pore size increased. Acidic reagent and submerged methodology were the best combination for fully dense Ti substrates. Hence, they were also employed for porous Ti substrates. Depending on the porosity of the substrates, variations can be observed both in the size and degree of agglomeration of the deposited AgNPs, entailing differences in the antibacterial behavior of the samples.

Keywords: porous titanium; silver nanoparticles; biofunctionalized titanium; antibacterial properties

Citation: Gaviria, J.; Alcudia, A.; Begines, B.; Beltrán, A.M.; Rodríguez-Ortiz, J.A.; Trueba, P.; Villarraga, J.; Torres, Y. Biofunctionalization of Porous Ti Substrates Coated with Ag Nanoparticles for Potential Antibacterial Behavior. *Metals* **2021**, *11*, 692. https://doi.org/10.3390/met11050692

Academic Editor: Maria Richert

Received: 11 March 2021
Accepted: 21 April 2021
Published: 23 April 2021

1. Introduction

The use of prosthetic solutions helps to overcome the limitations of people who have suffered trauma, accidents, or illnesses and are designed to meet functional or aesthetic requirements of the missing or damaged body part [1]. In this sense, its variety and complexity have increased dramatically in the last decades because of a rise in life expectancy and quality of life [2]. This social demand has turned this area into a growing business giving biomaterials for prosthetic applications a critical role in the search for new devices in biomedicine. In this sense, the utilization of materials like metals for healing was an early practice stretching back thousands of years. However, the use of metal implants was first introduced in 1895 by Lane as a metal plate for bone fracture [3]. Unfortunately, at this point all prostheses faced critical problems related to early corrosion or insufficient strength capabilities that were solved in part due to the introduction of stainless steel in 1920s, which had far superior corrosion resistance [4]. Significantly, for biomedical purposes, it is mandatory to evaluate the performance of the type of metal in terms of strength, resistance to fracture, biocompatibility, or stiffness depending on the specific implant or prosthesis application.

That said, ceramics, polymers, composites, or even titanium (Ti)-based alloys have been widely used for hard and soft tissues replacements. In particular Ti prostheses,

despite being more expensive, have shown better biological compatibility, which could be improved if needed, mechanical performance, and resistance to corrosion in cases of bone replacements, compared to other materials [5,6]. In addition, Ti is featured by its light weight or density (4.5 g/cm^3) compared to 7.9 g/cm^3 for 316 stainless steel and 8.3 g/cm^3 for cast CoCrMo alloys. Ti6Al4V is known for its excellent pitting corrosion resistance, tensile strength, biocompatibility, and excellent mechanical requirements [7]. Nevertheless, the high values of Young's modulus presented by fully dense Ti may show stress shielding that often evolves into bone resorption of the tissue surrounding the implant [8]. At this point, powder metallurgy is a technique that can control the amount and morphology of Ti porosity via a space-holder technique to produce complex porous structures that promote bone-in-growth, always associated with a low Young's modulus material. Furthermore, although Ti is an inert material, it does not have a desirable biofunctionality such as bone conductivity, bioactivity, blood compatibility, or therapeutic activity to inhibit infections produced by microbial adhesion, which leads to a poor osseointegration and, therefore, a potential implant loss. Unfortunately, between 5 and 10% of Ti implants have failures due to poor osseointegration promoted by biomechanical malfunction and/or bacterial infections [9]. Thus, it is necessary to develop solutions that minimize the risk of stress shielding and infections appearance in the implant area and their critical complications. In this sense, the use of porous Ti has been widely investigated as a potential solution to reduce stress-shielding issues [10–13]. Different techniques to fabricate these types of porous materials have been reported in the literature, such as powder metallurgy, foaming technologies, and additive manufacturing methods [14–22]. In addition, the potential use of β-Ti alloys has been explored to minimize the stress-shielding issues [23].

On the other hand, numerous studies have been developed in the last decade to add proper prothesis coating such as ceramics [24–27], bioglasses [28–30], or biopolymers [31] to induce hydroxyapatite to regenerate bone conductivity or blood compatibility. Superficial modifications of implants at the micro- and nano-scale are of great interest as they show clear improvements in biocompatibility. They favor bone-in-growth toward the implant, while maintaining the mechanical requirements of cortical bone tissues. Among the different approaches described in the literature to prevent infections are the functionalization of the implant surface by modifying the chemistry of the surface, its morphology, or the application of coatings [9,32–34]. In all approaches, a preventive action is taken on the implant, avoiding the spread of infection in its initial stages (bacterial adhesion, biofilm formation, or even invasion by diffusion to other tissues).

In the last decade, the nanotechnology in the field of medicine has been revolutionizing the way certain diseases are treated or detected since many novel techniques involving applications of nanoparticles are making remarkable progress in areas such as medicine [35] where they are designed to interact with tissues or cells with a high functional specificity that integrates biology and technology [36]. Nanoparticles (NPs) are particles of matter within the range of nanometers in diameter, with a high surface-to-volume ratio, good stability in general, and facile surface modification [37,38]. Among applications in medicine currently being developed are drug delivery (NPs are attracted to diseased cells, which allow direct treatment to reduce damage to healthy cells in the body), diagnostic/theragnostic techniques (allows for earlier detection treatment of the disease), or antibacterial treatment. Thus, NPs are useful chemical entities with interesting pharmacological characteristics applied when conventional treatments fail for any reason. In recent years, NPs based in metals or metal oxides have been described such as Ag [39–41], Au [42,43], Cu [44], CuO [45], or ZnO [46]. From these NPs, silver NPs (AgNPs) are known to damage bacterial cell via prolonged delivery of Ag+ ions, showing a potent antimicrobial activity [47] and a low cytotoxicity [48], and have better physiochemical and biological properties beyond bulk silver [49]. The action mechanism reported involves the anchorage of AgNPs to the bacterial cell previously to infiltration, causing physical charges modifications that lead to membrane damage, inducing reactive oxygen species (ROS) generation that provokes not only cellular contents leakage but also bacterial death via an apoptosis-like response.

Interestingly, AgNPs clinical treatment avoids the phenomenon called antibiotic resistance that happens when the human body develops the ability to defeat the drugs designed to kill them; therefore, alternative clinical treatments involving this therapeutically moieties are critical and desirable [50,51], such as the combination including antibacterial protection by phosphate or hydroxyapatite coatings implemented with AgNPs [52,53]. Another example is the use of porous or nanotubular matrices containing this type of nanoparticles [54,55]. Hence, the global rise of antibiotic resistance and the lack of new antibiotics open a new research era including metal-based antimicrobial therapies which is moving toward clinical studies. Although the benefits of the combination of antibacterial coatings of AgNPs onto Ti substrates have been previously reported in the literature [56], this study is based on a novel combination of a chemically functionalized porous Ti substrate with a potentially therapeutic coverture to implement mechanical and pharmacological characteristics. In this sense, the main aim for this investigation was the fabrication, by the space-holder technique, and the characterization of superficially modified porous Ti samples. These substrates presented a potential biomechanical and biofunctional balance, which guaranteed the requirements of the cortical bone tissue, while the proposed functionalization of the surface treatment was expected to improve the antibacterial behavior, particularly with the deposition of AgNPs.

2. Materials and Methods

The summary workflow of this investigation comparing fully dense, as a reference, and porous Ti samples and the AgNPs synthesis is shown in Figure 1. Furthermore, two different approaches to the biofunctionalization treatments were carried out, either acid or basic hydroxylation, and afterwards, AgNPs were both independently deposited on fully dense and porous Ti discs, to select the best choice between an "in situ" or "submerged" methodology. Substrate manufacturing details, surface modification treatments, microstructural characterization, and antibacterial behavior of the modified discs are described along the following sections.

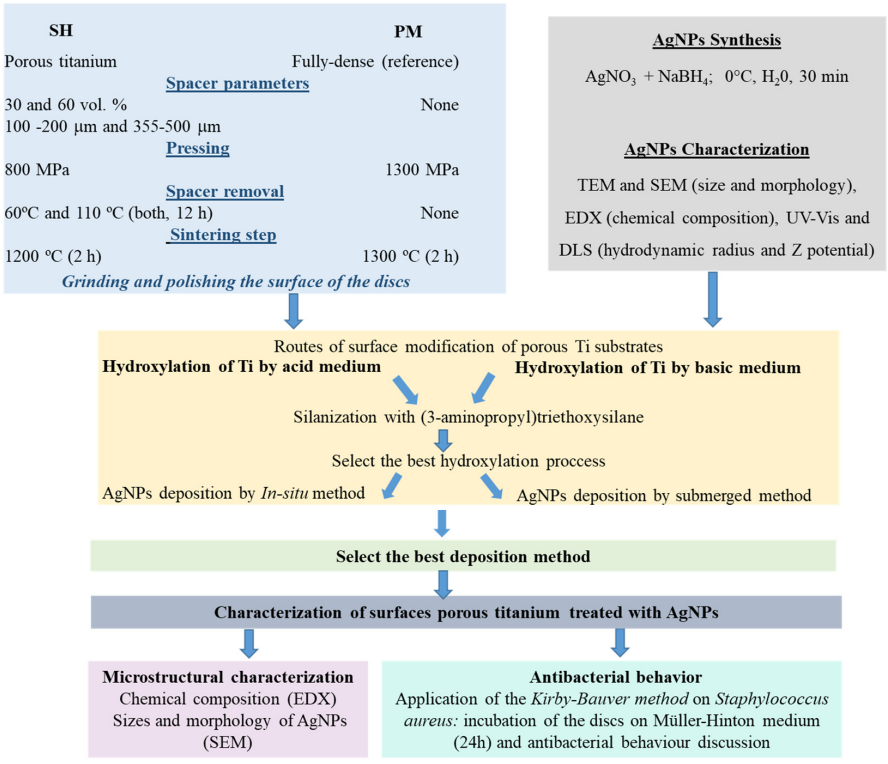

Figure 1. Scheme of the workflow of the study conducted in this investigation.

2.1. Fabrication and Characterization of the Ti Substrates

Commercial pure titanium powder (c.p. Ti) grade IV [57] with a mean particle size of $d_{[50]}$ = 23.3 µm [58], provided by SEJONG Materials Co. Ltd. (Seoul, Korea), was used in this study to obtain two types of substrates: fully dense and porous substrates. Fully dense substrates were fabricated by conventional powder metallurgy technique, using an Instron 5505 universal testing machine (Instron, UK) for pressing at 1300 MPa and then, sintering in a molybdenum chamber furnace (Termolab–Fornos Eléctricos, Lda., Águeda, Portugal) at 1300 °C for 2 h, in a high-vacuum condition (10^{-5} mbar). On the other hand, porous substrates were obtained by the space-holder technique, using as spacer particles 30 and 60 vol.% of ammonium bicarbonate (NH_4HCO_3), (BA), with a purity of 99%, supplied by Cymit Química S.L. (Barcelona, Spain), and two ranges in size (100–200 µm and 355–500 µm). The spacer particles and c.p. Ti powder were mixed, and once the blend was homogeneous (Turbula® T2C Shaker-Mixer, Basel, Switzerland for 40 min), it was pressed at 800 MPa with the same equipment. Then, the BA was removed in an oven at 10^{-2} mbar: firstly, at 60 °C for 12 h and secondly, at 110 °C for 12 h more. Finally, the porous green discs were also sintered in a molybdenum chamber furnace at 1250 °C for 2 h, in a high-vacuum condition (10^{-5} mbar). The manufactured discs presented an approximate average diameter of 11.9 and 2 mm of thickness.

The porosity of all obtained substrates was studied by Archimedes' method and Image analysis (IA). The equivalent pore diameter, pore shape factor, and total and interconnected porosity (D_{eq}, F_f, P_T, and P_i, respectively) [59] were evaluated by these methods. The shape factor was defined as $F_f = 4\pi A/(PE)^2$, where A is the area of the pore and PE is its experimental perimeter. Furthermore, the total area occupied by the micropores (less than 50 µm), macropores (associated with the spacer particles used), and the flat area of remaining Ti were evaluated using the image analysis software and with at least five pictures of 5× for each type of substrate. Finally, the mechanical behavior of the porous substrates (dynamic Young's modulus, E_d, yield strength, and σ_y), was estimated from the experimental porosity results (at least three measurements for each processing condition) and using fit equations reported in the literature [60].

2.2. Synthesis and Characterization of the AgNPs

AgNPs were obtained using the methodology proposed by Lee and Melsel [61], which consisted of dissolving $AgNO_3$ (2 mM) in deionized water. Under a continuous stirring at 115 rpm and 0 °C, $NaBH_4$ (1 vol.%) was added, and the mixture was left reacting for 30 min [62,63]. A yellowish suspension of AgNPs was obtained. Chemicals and solvents were purchased from Aldrich Chemicals Co (Madrid, Spain) and were used without further purification.

UV-Vis absorbance spectroscopy was used to corroborate the presence of AgNPs. Measurements were carried out in an Agilent Cary 5000 spectrophotometer at 298 K from 300 to 600 nm with a wavelength accuracy of ±0.3 nm and a spectral bandwidth of 0.5 nm. In order to check the quality (size distribution and composition) of the AgNPs, they were characterized by dynamic light scattering (DLS) using a NanoSizer Nano ZS® (Malvern Panalytical, UK) and a scanning electron microscopy (SEM) using a JEOL, JSM 6490-LV (Tokio, Japan). Compositional analyses were performed by energy dispersive spectroscopy (EDS) coupled to the scanning electron microscope (EDS-SEM). In addition, transmission electron microscope techniques (TEM) were performed on a FEI Tecnai G2 F20 (FEI, Eindhoven, The Netherlands). For TEM studies, a drop of the solution was deposited on an ultrathin carbon film on a nickel grid.

2.3. Modification and Characterization of the Surface of the Ti Substrates

In this work, concerning the Ti surface modifications, two alternative hydroxylation treatments were evaluated: a basic treatment, consisting of a conventional chemical etching with a NaOH solution [64,65], and acid treatment by the exposing the Ti surface to concentrated oxidant sulfuric acid, ("piranha solution", H_2O_2/H_2SO_4) [66,67]. To perform

the attack treatment, either with the basic medium or with acid medium, the Ti samples were soaked in 5 M NaOH at 60 °C for 24 h or with the "piranha solution" at 75 °C (acid solution: 30% H_2O_2 and 70% H_2SO_4) for 1.5 h, respectively. Next, after the basic or acid treatments, all samples were subjected to excessive washing with milli-Q water and were completely dried with a nitrogen stream. Then, the hydroxyl groups in Ti surface attacked and displaced the alkoxy groups on the silane to form a covalent O-Si- bond via a silanization reaction, immersing them in a solution of (3-aminopropyl)triethoxysilane (APTES) at 1% (*v*/*v*) for 15 min, under constant stirring, followed by a heat treatment in a conventional drying oven (BINDER®, BINDER GmbH, Tuttlingen, Germany) with convective air at 115 °C for 1.5 h. Additionally, three washes were carried out to rinse out with water and, finally, to dry it with a stream of nitrogen.

Once the best hydroxylation treatment (basic or acid treatment) was chosen in terms of the best homogenization and roughness of the surface followed by a posterior silanization, this study also evaluated as a second implementation two different routes of AgNPs deposition on the hydroxylated Ti surfaces. On the one hand, the synthesis of the AgNPs was performed in the presence of the Ti substrates, and it was called "in situ" synthesis. On the other hand, the suspension of AgNPs was previously obtained, and then, the Ti substrates were submerged in such solution, calling this method "submerged".

The modified surface of the Ti discs was then characterized by different techniques; microstructural features (morphology, roughness, and AgNPs distribution) were studied using a scanning electron microscopy (SEM, JSM 6490-LV by Jeol, Japan), while the chemical composition was analyzed by energy dispersive spectroscopy (EDS) couple to the SEM microscope (EDS-SEM).

Moreover, the antibacterial behavior of AgNPs-coated samples was evaluated following the Kirby–Bauer disc-diffusion method [68] against *Staphylococcus aureus* (ATCC 25923) as bacterial model. Petri dishes containing Mueller–Hinton medium were covered with a suspension of bacteria (104 CFU/mL) using a sterile hyssop. Immediately afterward, the modified surface of the Ti discs was deposited on top of the seeded medium. Samples were incubated at 37 °C for 24 h in aerobic conditions. Inhibition halos were measured using ImageJ software. For statistical analysis, at least three measurements in three samples were taken for n = 9 of the different Ti discs.

3. Results and Discussion

The microstructural characterization (porosity parameters) of the uncoated titanium substrates using the Archimedes' method and image analysis, as well as the mechanical properties estimated from the these experimentally values [60,69], are summarized in Table 1.

Table 1. Experimental porosity parameters and estimation of the mechanical properties.

		Microstructural Characterization				Estimated Mechanical Behavior	
		P_T (%)	P_i (%)	D_{eq} (μm)	Ff	E_d (GPa)	σ_y (MPa)
Fully dense		2.4 ± 0.3	1.3 ± 0.3	5 ± 3	0.97 ± 0.1	103.1 ± 1.0	580 ± 3
30 vol.%	100–200 μm	30.2 ± 0.2	18.1 ±0.1	192 ± 117	0.72 ± 0.2	56.8 ± 0.7	354 ± 6
	355–500 μm	30.1 ± 0.1	19.0 ± 0.1	435 ± 401	0.75 ± 0.1	57.0 ± 1.4	341 ± 7
60 vol.%	100–200 μm	56.4 ± 0.5	51.8 ± 1.3	259 ± 287	0.74 ± 0.1	32.3 ± 0.6	88 ± 4
	355–500 μm	57.8 ± 0.5	53.0 ± 0.9	295 ± 331	0.77 ± 0.3	31.3 ± 1.5	80 ± 5

The pore sizes and contents obtained corroborate the effectiveness of the use of the space-holder technique. The pores size depends both on the size of the spacer applied and on the potential coalescence phenomena. This fact is particularly critical on substrates with higher pore content and/or smaller sizes. From the data shown in Table 1, it can be seen that the pores obtained by the conventional power metallurgy (PM) route are more rounded (pore shape factor values closer to 1) than those obtained with the spacers technique. On

the other hand, as expected, there is an inverse relationship between the pore content and the mechanical properties (stiffness and yield strength) of titanium substrates.

In general, it has been considered that there are two types of pores: one of them due to the spacer used (content and size) and the other inherent to the sintering conditions. In this sense, pore diameters greater than 50 μm have been identified as macropores and less than 50 μm as micropores. The percentage of area occupied by each one of them, over the total titanium discs surface (2.835 mm^2), are shown in Table 2. In general, a clear relation can be established between the area occupied by macropores and the probability to occur biggest defect (macropore that controls cracking). In this context, as detailed in this discussion later, the role played by pores and the titanium flat zone in bacterial behavior could also be evaluated.

Table 2. Distributions occupied area of titanium discs surface obtained by image analysis: flat area, macropores and micropores.

Fully Dense		Flat Area (%)	Macropores Area (%)	Micropores Area (%)
		98.45	**0**	**1.65**
30 vol.%	100–200	68.96	30.48	0.56
	355–500	72.82	26.74	0.43
60 vol.%	100–200	60.36	39.46	0.17
	355–500	40.77	59.00	0.22

Note: all measurement errors were lower than 0.01%.

To achieve an efficient deposition through chemical stabilization of AgNPs on the substrate, the Ti surface was first treated with basic or acidic solutions (NaOH or piranha, respectively) and later modified with the chemical linker APTES via a silanization reaction to form strong covalent bonds and to introduce the necessary amino terminal moieties. The successful interaction between free primary amino groups (-NH_2) from APTES and AgNPs has been widely demonstrated in the literature [70,71]. Figure 2 shows the images of the chemically etched surfaces, as well as the chemical composition spectra obtained by EDS, of porous Ti substrates. Interestingly, it is observed that the surfaces modified with the NaOH treatment presented a much greater degradation compared to the piranha treatment, since the first one induces a more pronounced material loss as well as a critical increase of numerous irregularities on the material surface. This eroded morphology could provoke a potential steric obstruction impeding an efficient cell adhesion and therefore a partial antibacterial effect. At the same time, it is worth mentioning that a flatter surface promotes the presence of silver nanoparticles and consequently guarantees a greater bactericide effect; therefore, the balance of these two behaviors should be taken into consideration.

On the other hand, the synthesis of AgNPs employed a strong reducing agent as $NaBH_4$ and low temperatures. Figure 3 collects the main results related to the synthesis and characterization of AgNPs, emphasizing the spherical morphology, size distribution, and the spectrophotometry study of the particle suspension stability. The presence of AgNPs in suspension was confirmed by the appearance of a wide band centered at 387 nm in the UV-Vis, while the mean particle size estimated by TEM was 16 nm.

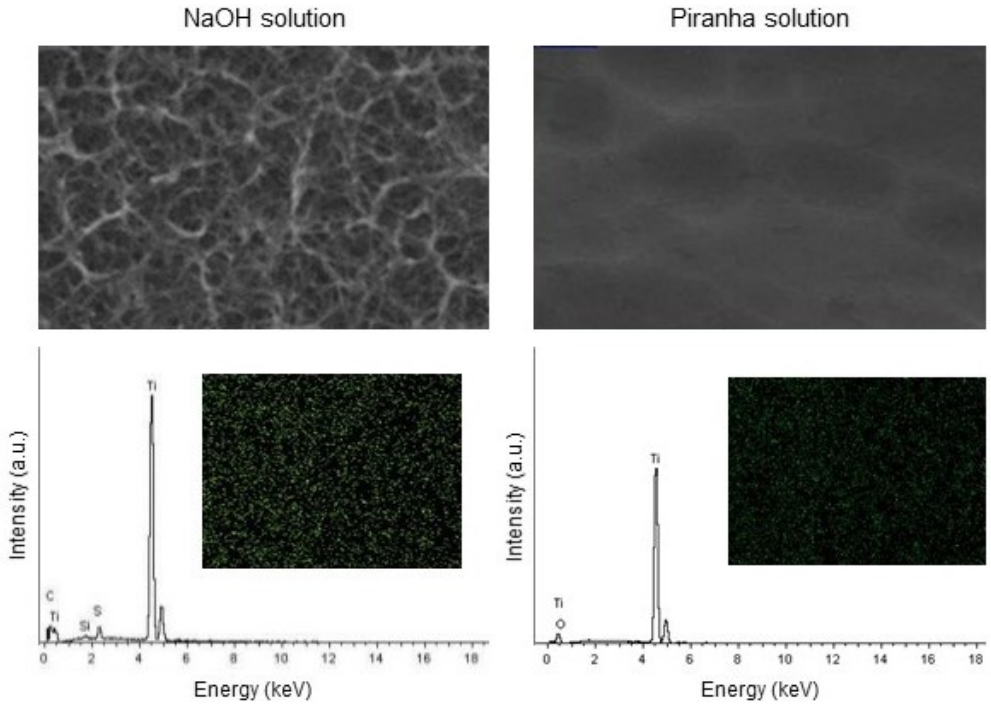

Figure 2. SEM micrographs and EDS-SEM of fully dense Ti substrates, after etching with NaOH or piranha reagents.

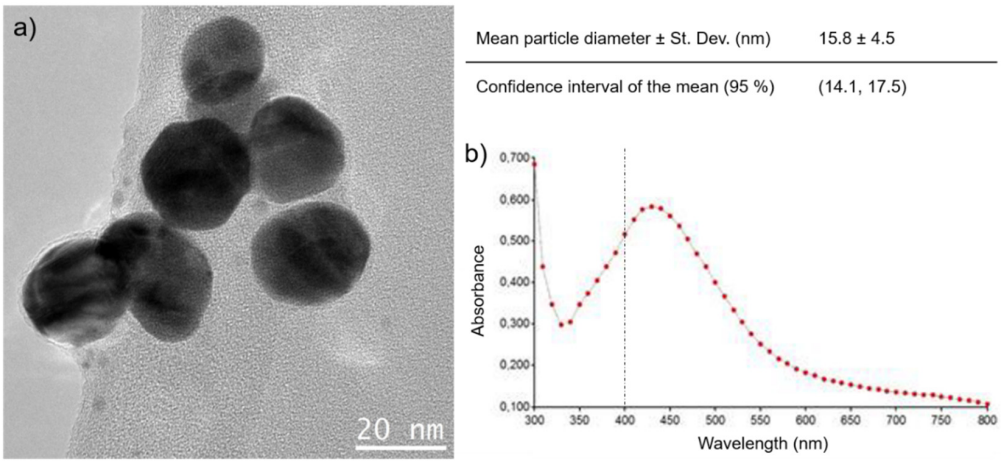

Figure 3. Characterization of AgNPs, (**a**) TEM experiment showing particle's morphology, size distribution, and (**b**) spectrophotometry study of the particle suspension stability.

However, two different deposition methods were attempted: "submerged", in which the synthesis reaction was conducted prior to the substrate submersion in the nanoparticle suspension; and "in situ", in which the substrate is submerged in the reaction mixture before adding the $AgNO_3$, inducing the nanoparticle synthesis directly on top of the substrate surface. These different deposition mechanisms lead to small differences in the AgNPs characteristics. Thus, the particles obtained by NaOH (119.5 nm) are slightly bigger than the ones prepared by the piranha treatment (116.2 nm), as displayed in Table 3, both measured by DLS. The observation of the zeta potential (ZP) shows key differences for the colloidal system obtained from the "submerged" compared to the "in situ" AgNPs methodology. It is worthy to mention that, in general, the most stable nanoparticle colloidal solutions are in the range of less than −30 mV or values greater than +30 mV. In our case, the observed zeta potential values for both acid or basic treatments indicate that the

colloidal suspension of Ag reached values of −29.6 mV and −36.4 mV at 25 °C, respectively, evidencing a colloidal AgNPs system with stable regions.

Table 3. Chemical reduction parameters of AgNPs at 25 °C.

Ti Hydroxylation	ZP (mV)	Mean Diameter (nm)	PdI	pH
acid medium	−29.6	116.2	0.332	7
basic medium	−36.4	119.5	0.402	7

3.1. Characterization of Surfaces of Ti Substrates with AgNPs

Figure 4 shows the EDS spectra corresponding to the surfaces of the fully dense Ti substrates pretreated first with the piranha reagent and after silanized and coated with AgNPs, using the two different deposition routes previously described (immersion and "in situ"). Significantly, the EDS results indicate the presence of titanium and silver primarily. A higher concentration of Ag deposited on the surface of the titanium discs immersed in the nanoparticle suspension is observed compared to the one obtained with the "in situ" method. Unfortunately, the method of disc immersion in the suspension causes agglomerates of AgNPs. The opposite case was observed during the elaboration of colloidal systems with the "in situ" method, where reduction in the size of AgNPs was noted. Pris and Krzysztof et al. [72] reported the impact of a vigorous stirring during the suspension (degree and time) not only on the color but also to prevent agglomeration of the AgNPs. In this sense, authors recommend implementing vigorous shaking for times less than 30 min. In their study, they observed a direct relationship between the stirring time vs. the agglomeration of the AgNPs and the dark color of the suspension. Furthermore, the presence of agglomerates of AgNPs can be detected in the study shown in Figure 5, independent of the functionalization treatment carried out on the surface of the fully dense titanium substrate (NaOH or piranha). Considering the best semiquantitative results previously discussed corresponding to the surfaces of the fully dense Ti substrates, from this moment on, this work only takes into account the combination of etching with the piranha reagent and the "immersion" methodology for AgNPs deposition to modify the surface of porous titanium substrates as the best procedure.

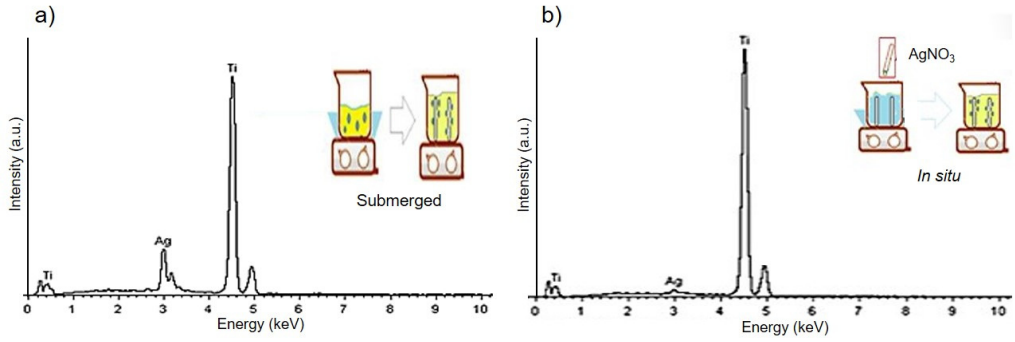

Figure 4. EDS spectra of the Ti surfaces coated with AgNPs using two routes of deposition (**a**) submerged reduction and (**b**) "in situ" reduction.

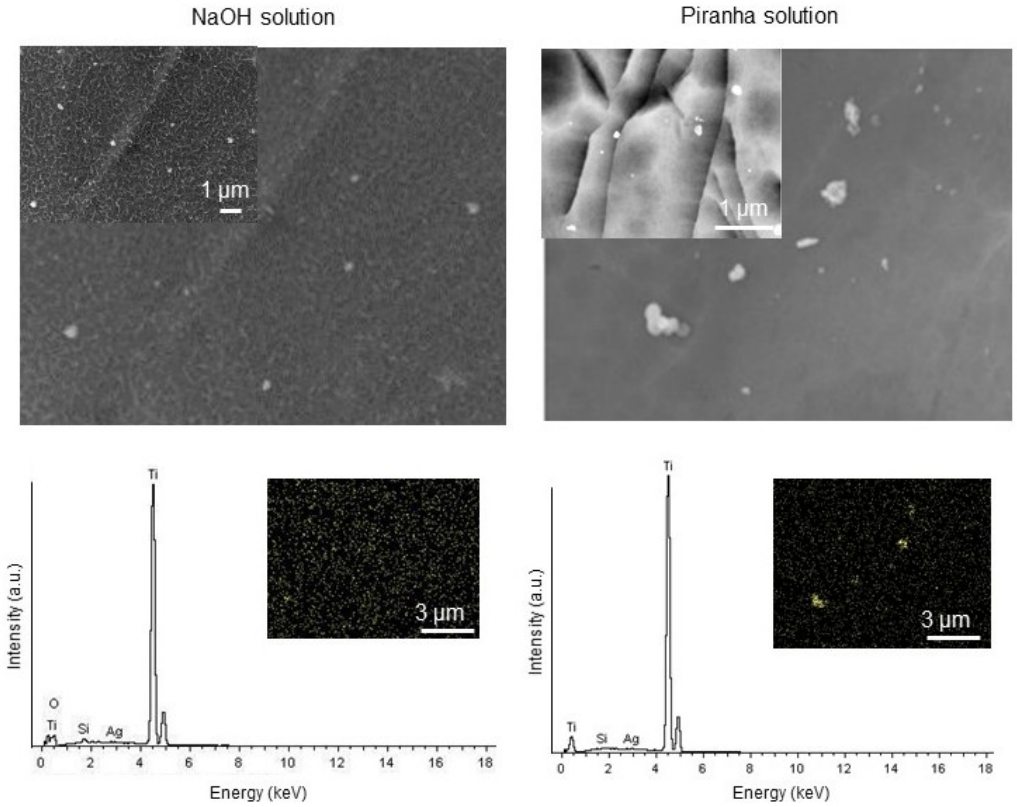

Figure 5. SEM micrographs and EDS-SEM of fully dense Ti substrates, treated with NaOH (**left**), or piranha (**right**), and after coating with AgNPs via a "submerged" reduction in both cases.

Once the surface modification methodology was optimized on fully dense Ti substrate, the surface functionalization was studied in porous substrates. Figure 6 shows images obtained by SEM of the modified surface (AgNPs deposition by the immersion method, after etching with piranha treatment) of the porous titanium substrates obtained with different content and spacer size range. In general, it can be observed that AgNPs are mainly deposited on the flat area between the pores but in lower degree on the inner surface of them. This would entail a higher AgNP content in the samples with 30 vol% of pores, since they have larger flat area where AgNP can attach to than the substrates with 60 vol%, as displayed in Table 2. In addition, depending on the porosity of the substrates, differences can be observed both in the size and degree of agglomeration of the deposited AgNPs, as well as in the homogeneity of their distribution. In this sense, smaller AgNPs are obtained for the 60 vol.% and the smallest spacer size range (100–200 µm), while the presence of nanoparticle agglomerates is greater for the substrates obtained with larger spacer sizes. The reason for this behavior is not so clear, but it could be related to the differences in the dip deposition process, depending on the flat area of titanium (surface wettability). As discussed later, the conjunction of these effects has a direct influence on the antibacterial behavior of the samples. Thus, although the substrates with 30 vol% of pores show greater absolute antibacterial inhibition due to a larger flat surface where AgNP can attach to, samples with 60 vol% present greater relative antibacterial inhibition due to a higher NP agglomeration.

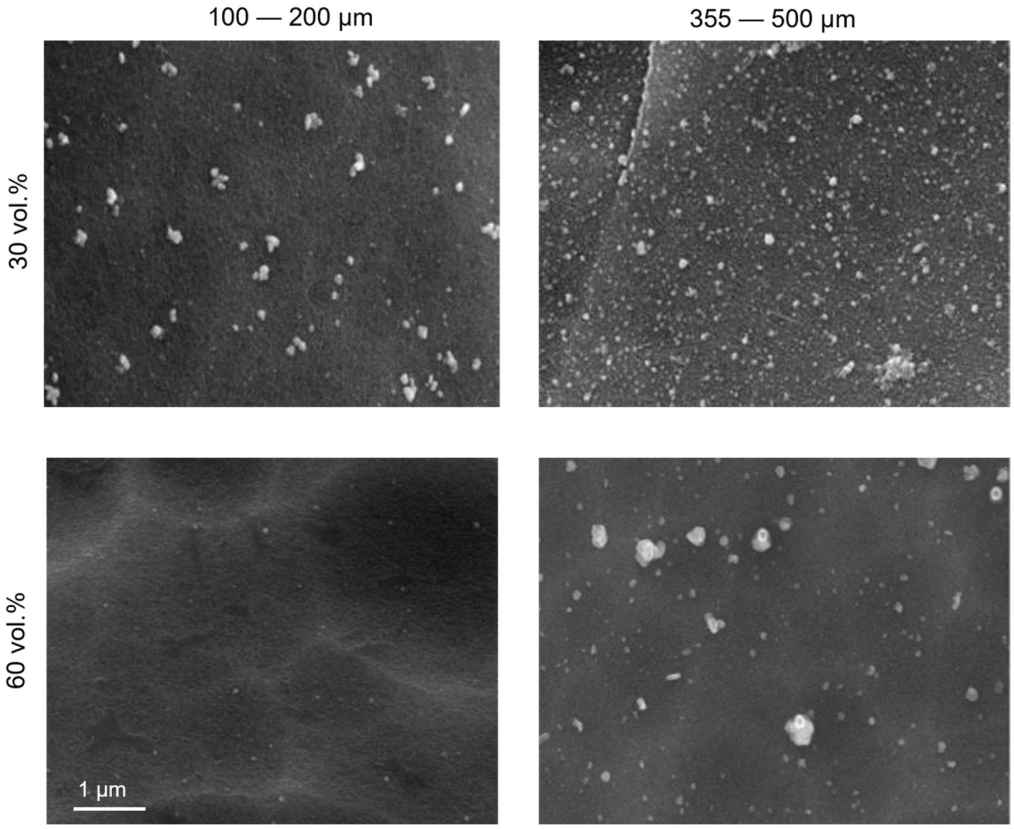

Figure 6. SEM of flat area of porous Ti substrates coated with AgNPs. Influence of the content and range of pore sizes. Note: all surfaces have previously been attacked with piranha. In addition, white contrast corresponds to agglomerated AgNPs.

3.2. Characterization of the Antibacterial Behavior of Ti Substrates

For the reasons stated above, the study of antibacterial behavior was carried out on discs superficially modified (hydroxylated) with the piranha reagent followed by silanization and then submerged in the suspension of silver nanoparticles. To demonstrate the effectiveness of AgNPs coating, a qualitative experiment of bacterial growth inhibition was conducted using *Staphylococcus aureus* as a Gram+ bacterial model [73]. Initially, tests were performed on fully dense discs comparing the antimicrobial effect on only silanized samples and samples with a silanization and AgNP-coating treatment. Once the antibacterial character of these substrates was confirmed, the same experiments were carried out on porous samples, considering both pore samples (30 and 60 vol.%) as well as both pore size ranges (100–200 and 355–500 µm). Additionally, the samples were studied and compared with only silanization treatment (as blank sample) and the ones with silanization followed by AgNPs coating. As expected, none of the samples with just the silanization treatment presented any inhibition halo. In general, in porous substrates, independent of pore density and pore size distribution, all samples displayed antibacterial behavior (Figure 7a), although they were lower than the one displayed by the fully dense substrate. In the particular case of porous samples, those ones containing a 30 vol.% of porosity presented slightly higher bacterial inhibition than the ones with a 60 vol.% of porosity in absolute terms, probably due to a higher concentration of AgNPs related to a larger flat Ti surface where they can get attached. To prove this, a study of the surface of the different sample was conducted: a quantitative evaluation including flat areas, macropore areas and micropore areas were included, considering only micropores as those with a diameter smaller than 50 µm. Hence, the flat area proportion of the samples (calculated from a total titanium discs surface of 2.835 mm^2, considering an ideal fully dense substrate without micropores) (Table in Figure 7b), where the AgNPs can attach easily, was higher

for the substrates with 30 vol.% of porosity than the flat area of those samples with higher porosity. Therefore, in total, the substrates of lower porosity presented higher amounts of Ag. However, if a relation between the inhibition area and the flat surface of each sample is carried out, the results revealed that the relative inhibition was more pronounced for the substrates with 60 vol.% of porosity, probably due a higher content of AgNPs, both inside the pores and agglomerated in the flat area (as above revealed by SEM) that compensate the lower amount of Ag corresponding to the flat area.

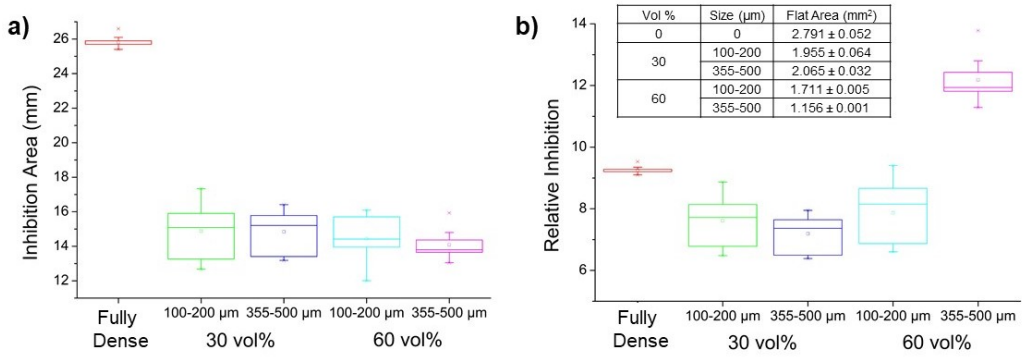

Figure 7. Antibacterial behavior showed by AgNPs-coated Ti substrates, considering (**a**) the total inhibition area obtained for each substrate and (**b**) the relative inhibition related to the flat area of each type of sample (flat surface calculated from a total titanium discs surface of 2.835 mm^2, considering an ideal fully dense substrate without micropores).

These results are consistent with the total inhibition area observed in a sample with 40% porosity recently reported by our group [56]. This inhibition area is located between the inhibition area obtained for samples with 30 and 60 vol.% porosity. In comparison, previously reported results by Jingchao et al. [51], concerning the evaluation of inhibition halos of fully dense Ti coated with AgNPs showed negligible zones of inhibition due to a low concentration of silver ions in the surrounding environment.

Finally, no statistical analyses concerning the antibacterial studies have been developed as limitations of the study; a more accurate way to evaluate this effect for future studies should be carried out involving CFU data.

4. Conclusions

This study is based on a novel combination of a chemically functionalized porous Ti substrate with a potentially therapeutic coverture AgNPs. The absolute antibacterial activity of fully dense samples is higher than those showed by the porous materials. However, the high difference on the stiffness between the implant and the cortical bone tissue compromises the clinical success (resorption of the bone surrounding the implant). The superficially modified porous implants presented in this work showed an improved biomechanical and biofunctional balance, achieving at the same time, a reduction of the stress shielding, allowing the bone-in-growth and better antibacterial behavior. In this context, the main conclusions are as follows: (1) It culd be generally observed that mechanical resistance decreases by increasing the size of the pores, for similar pore content. (2) To achieve an efficient deposition through chemical stabilization of AgNPs on the substrate, the Ti surface was first treated with basic or acidic solutions (NaOH or piranha, respectively) and later modified with the chemical linker APTES via a silanization reaction. (3) Interestingly, it was observed that the surfaces modified with the NaOH treatment presented a much greater degradation compared to the piranha treatment. (4) The synthesis of AgNPs employed a strong reducing agent as $NaBH_4$ and low temperatures. Two different deposition methods were attempted: "submerged" and "in situ". Considering the best semiquantitative results previously discussed corresponding to the surfaces of the fully dense Ti substrates, the best combination of etching was piranha reagent and the

"immersion" methodology for AgNPs deposition. (5) For porous Ti substrates, differences could be observed both in the size and degree of agglomeration of the deposited AgNPs. In particular, those using a 30 vol.% as a spacer presented slightly higher bacterial inhibition than the ones with a 60 vol.% as a spacer in absolute terms, probably due to a higher concentration of AgNPs related to a larger flat Ti surface where they can get attached. However, if a relation between the inhibition area and the flat surface of each sample is carried out, the results revealed that the relative inhibition was more pronounced for the substrates with 60 vol. % as spacer, probably due a higher content of AgNPs both inside the pores and agglomerated in the flat area that compensate the lower amount of Ag corresponding to the flat area.

Author Contributions: Conceptualization, J.V. and Y.T.; investigation, J.G.; writing—original draft preparation, A.A., B.B., A.M.B., J.A.R.-O. and P.T.; writing—review and editing, A.A., B.B., A.M.B., J.A.R.-O., P.T. and Y.T.; supervision and project administration, J.V., A.A. and Y.T. All authors have read and agreed to the published version of the manuscript.

Funding: This work was supported by the Ministry of Science and Innovation of Spain under the grant PID2019-109371GB-I00, by the Junta de Andalucía–FEDER (Spain) through the Project Ref. US-1259771 and by the Junta de Andalucía-Proyecto de Excelencia (Spain) P18-FR-2038.

Data Availability Statement: Not applicable.

Acknowledgments: The authors dedicate this paper to the memory of Juan J. Pavón Palacio (University of Antioquia, Colombia). They also thank Freimar Segura, Juan Guillermo Castaño, and Durley Eliana Restrepo for their support in bacterial tests. This work was supported by the Ministry of Science and Innovation of Spain under the grant PID2019-109371GB-I00, by the Junta de Andalucía–FEDER (Spain) through the Project Ref. US-1259771 and by the Junta de Andalucía-Proyecto de Excelencia (Spain) P18-FR-2038.

Conflicts of Interest: The authors declare no conflict of interest.

References

1. Couqueberg, Y.; Augoyard, R.; Augoyard, M.; Berry-Kromer, V.; Bouby, C.; Girod, L. A statistical study of metatarsal anatomy: Toward the design of wide-range prosthetic solutions. *Foot Ankle Spec.* **2017**, *11*, 277–287. [CrossRef]
2. Chadwell, A.; Diment, L.; Micó-Amigo, M.; Morgado Ramírez, D.Z.; Dickinson, A.; Granat, M.; Kenney, L.; Kheng, S.; Sobuh, M.; Ssekitoleko, R.; et al. Technology for monitoring everyday prosthesis use: A systematic review. *J. Neuroeng. Rehabil.* **2020**, *17*. [CrossRef]
3. Bartoníbek, J. Early history of operative treatment of fractures. *Arch. Orthop. Trauma Surg.* **2010**, *130*, 1385–1396. [CrossRef]
4. Bekmurzayeva, A.; Duncanson, W.J.; Azevedo, H.S.; Kanayeva, D. Surface modification of stainless steel for biomedical applications: Revisiting a century-old material. *Mater. Sci. Eng. C* **2018**, *93*, 1073–1089. [CrossRef] [PubMed]
5. Lascano, S.; Arévalo, C.; Montealegre-Melendez, I.; Muñoz, S.; Rodriguez-Ortiz, J.A.; Trueba, P.; Torres, Y. Porous titanium for biomedical applications: Evaluation of the conventional powder metallurgy frontier and space-holder technique. *Appl. Sci.* **2019**, *9*, 982. [CrossRef]
6. Sidambe, A. Biocompatibility of advanced manufactured titanium implants—A review. *Materials* **2014**, *7*, 8168–8188. [CrossRef]
7. González, J.E.; De Armas, G.; Negrin, J.; Beltrán, A.M.; Trueba, P.; Gotor, F.J.; Peón, E.; Torres, Y. Metals influence of successive chemical and thermochemical treatments on surface features of Ti6Al4V samples manufactured by SLM. *Metals* **2021**, *11*, 313. [CrossRef]
8. Civantos, A.; Beltrán, A.M.; Domínguez-Trujillo, C.; Garvi, M.D.; Lebrato, J.; Rodríguez-Ortiz, J.A.; García-Moreno, F.; Cauich-Rodriguez, J.V.; Guzman, J.J.; Torres, Y. Balancing porosity and mechanical properties of titanium samples to favor cellular growth against bacteria. *Metals* **2019**, *9*, 1039. [CrossRef]
9. Zhao, L.; Chu, P.K.; Zhang, Y.; Wu, Z. Antibacterial coatings on titanium implants. *J. Biomed. Mater. Res. Part B Appl. Biomater.* **2009**, *91*, 470–480. [CrossRef] [PubMed]
10. Pałka, K.; Pokrowiecki, R. Porous titanium implants: A review. *Adv. Eng. Mater.* **2018**, *20*, 1–18. [CrossRef]
11. Kaur, M.; Singh, K. Review on titanium and titanium based alloys as biomaterials for orthopaedic applications. *Mater. Sci. Eng. C. Mater. Biol. Appl.* **2019**, *102*, 844–862. [CrossRef]
12. Miao, X.; Sun, D. Graded/gradient porous biomaterials. *Materials* **2009**, *3*, 26–47. [CrossRef]
13. Betts, C. Benefits of metal foams and developments in modelling techniques to assess their materials behaviour: A review. *Mater. Sci. Technol.* **2012**, *28*, 129–143. [CrossRef]
14. Ryan, G.; Pandit, A.; Apatsidis, D.P. Fabrication methods of porous metals for use in orthopaedic applications. *Biomaterials* **2006**, *27*, 2651–2670. [CrossRef]

15. Kobatake, R.; Doi, K.; Kubo, T.; Makihara, Y.; Oki, Y.; Yokoi, M.; Umehara, H.; Tsuga, K. Novel fabrication of porous titanium by a resin-impregnated titanium substitution technique for bone reconstruction. *RSC Adv.* **2019**, *9*, 1625–1631. [CrossRef]
16. Zhang, X.Y.; Fang, G.; Leeflang, S.; Zadpoor, A.A.; Zhou, J. Topological design, permeability and mechanical behavior of additively manufactured functionally graded porous metallic biomaterials. *Acta Biomater.* **2019**, *84*, 437–452. [CrossRef]
17. Bari, K.; Arjunan, A. Extra low interstitial titanium based fully porous morphological bone scaffolds manufactured using selective laser melting. *J. Mech. Behav. Biomed. Mater.* **2019**, *95*, 1–12. [CrossRef]
18. Tan, X.P.; Tan, Y.J.; Chow, C.S.L.; Tor, S.B.; Yeong, W.Y. Metallic powder-bed based 3D printing of cellular scaffolds for orthopaedic implants: A state-of-the-art review on manufacturing, topological design, mechanical properties and biocompatibility. *Mater. Sci. Eng. C Mater. Biol. Appl.* **2017**, *76*, 1328–1343. [CrossRef] [PubMed]
19. Naebe, M.; Shirvanimoghaddam, K. Functionally graded materials: A review of fabrication and properties. *Appl. Mater. Today* **2016**, *5*, 223–245. [CrossRef]
20. Chen, Y.J.; Feng, B.; Zhu, Y.P.; Weng, J.; Wang, J.X.; Lu, X. Fabrication of porous titanium implants with biomechanical compatibility. *Mater. Lett.* **2009**, *63*, 2659–2661. [CrossRef]
21. Özbilen, S.; Liebert, D.; Beck, T.; Bram, M. Fatigue behavior of highly porous titanium produced by powder metallurgy with temporary space holders. *Mater. Sci. Eng. C* **2016**, *60*, 446–457. [CrossRef]
22. de Vasconcellos, L.M.R.; de Oliveira, M.V.; de Alencastro Graça, M.L.; de Vasconcellos, L.G.O.; Carvalho, Y.R.; Cairo, C.A.A. Porous titanium scaffolds produced by powder metallurgy for biomedical applications. *Mater. Res.* **2008**, *11*, 275–280. [CrossRef]
23. Sidhu, S.S.; Singh, H.; Gepreel, M.A.H. A review on alloy design, biological response, and strengthening of β-titanium alloys as biomaterials. *Mater. Sci. Eng. C* **2021**, *121*, 111661. [CrossRef]
24. Palanivelu, R.; Kalainathan, S.; Ruban Kumar, A. CERAMICS Characterization studies on plasma sprayed (AT/HA) bi-layered nano ceramics coating on biomedical commercially pure titanium dental implant. *Ceram. Int.* **2014**, *40*, 7745–7751. [CrossRef]
25. Yerokhin, A.; Parfenov, E.V.; Matthews, A. In situ impedance spectroscopy of the plasma electrolytic oxidation process for deposition of Ca- and P-containing coatings on Ti. *Surf. Coat. Technol.* **2016**, *301*, 54–62. [CrossRef]
26. Zhang, X.; Aliasghari, S.; Němcová, A.; Burnett, T.L.; Kuběna, I.; Šmíd, M.; Thompson, G.E.; Skeldon, P.; Withers, P.J. X-ray computed tomographic investigation of the porosity and morphology of plasma electrolytic oxidation coatings. *ACS Appl. Mater. Interfaces* **2016**, *8*, 8801–8810. [CrossRef]
27. Sobolev, A.; Zinigrad, M.; Borodianskiy, K. Ceramic coating on Ti-6Al-4V by plasma electrolytic oxidation in molten salt: Development and characterization. *Surf. Coat. Technol.* **2021**, *408*, 126847. [CrossRef]
28. Beltrán, A.M.; Begines, B.; Alcudia, A.; Rodríguez-Ortiz, J.A.; Torres, Y. Biofunctional and tribomechanical behavior of porous titanium substrates coated with a bioactive glass bilayer (45S5-1393). *ACS Appl. Mater. Interfaces* **2020**, *12*, 30170–30180. [CrossRef] [PubMed]
29. Beltrán, A.M.; Alcudia, A.; Begines, B.; Rodríguez-Ortiz, J.A.; Torres, Y. Porous titanium substrates coated with a bilayer of bioactive glasses. *J. Non-Cryst. Solids* **2020**, *544*, 120206. [CrossRef]
30. Domínguez-Trujillo, C.; Ternero, F.; Rodríguez-Ortiz, J.A.; Pavón, J.J.; Montealegre-Meléndez, I.; Arévalo, C.; García-Moreno, F.; Torres, Y. Improvement of the balance between a reduced stress shielding and bone ingrowth by bioactive coatings onto porous titanium substrates. *Surf. Coat. Technol.* **2018**, *338*, 32–37. [CrossRef]
31. D'almeida, M.; Amalric, J.; Brunon, C.; Grosgogeat, B.; Toury, B. Relevant insight of surface characterization techniques to study covalent grafting of a biopolymer to titanium implant and its acidic resistance. *Appl. Surf. Sci.* **2015**, *327*, 296–306. [CrossRef]
32. Shen, X.; Zhang, Y.; Ma, P.; Sutrisno, L.; Luo, Z.; Hu, Y.; Yu, Y.; Tao, B.; Li, C.; Cai, K. Fabrication of magnesium/zinc-metal organic framework on titanium implants to inhibit bacterial infection and promote bone regeneration. *Biomaterials* **2019**, *212*, 1–16. [CrossRef] [PubMed]
33. Ballarre, J.; Aydemir, T.; Liverani, L.; Roether, J.A.; Goldmann, W.H.; Boccaccini, A.R. Versatile bioactive and antibacterial coating system based on silica, gentamicin, and chitosan: Improving early stage performance of titanium implants. *Surf. Coat. Technol.* **2020**, *381*, 125138. [CrossRef]
34. Zhang, L.-C.; Chen, L.-Y.; Wang, L. Surface modification of titanium and titanium alloys: Technologies, developments, and future interests. *Adv. Eng. Mater.* **2020**, *22*, 1901258. [CrossRef]
35. Saini, R.; Saini, S.; Sugandha, S. Nanotechnology: The future medicine. *J. Cutan. Aesthet. Surg.* **2010**, *3*, 32–33. [CrossRef]
36. Emerich, D.F.; Thanos, C.G. Nanotechnology and medicine. *Expert Opin. Biol. Ther.* **2003**, *3*, 655–663. [CrossRef]
37. Shi, J.; Votruba, A.R.; Farokhzad, O.C.; Langer, R. Nanotechnology in drug delivery and tissue engineering: From discovery to applications. *Nano Lett.* **2010**, *10*, 3223–3230. [CrossRef]
38. Nasrollahzadeh, M.; Sajadi, S.M.; Sajjadi, M.; Issaabadi, Z. An Introduction to Nanotechnology. In *Interface Science and Technology*; Elsevier, B.V., Ed.; Academic Press: Cambridge, MA, USA, 2019; Volume 28, pp. 1–27.
39. Zhou, W.; Ma, Y.; Yang, H.; Ding, Y.; Luo, X. A label-free biosensor based on silver nanoparticles array for clinical detection of serum p53 in head and neck squamous cell carcinoma. *Int. J. Nanomed.* **2011**, *6*, 381–386. [CrossRef] [PubMed]
40. Arunachalam, R.; Dhanasingh, S.; Kalimuthu, B.; Uthirappan, M.; Rose, C.; Baran Mandal, A. Phytosynthesis of silver nanoparticles using Coccinia grandis leaf extract and its application in the photocatalytic degradation. *Colloids Surf. B Biointerfaces* **2012**, *94*, 226–230. [CrossRef]
41. Giljohann, D.A.; Seferos, D.S.; Daniel, W.L.; Massich, M.D.; Patel, P.C.; Mirkin, C.A. Gold nanoparticles for biology and medicine. *Angew. Chem. Int. Ed. Engl.* **2010**, *49*, 3280–3294. [CrossRef]

42. Begines, B.; Alcudia, A.; Aguilera-Velazquez, R.; Martinez, G.; He, Y.; Wildman, R.; Sayagues, M.-J.; Jimenez-Ruiz, A.; Prado-Gotor, R. Design of highly stabilized nanocomposite inks based on biodegradable polymer-matrix and gold nanoparticles for Inkjet Printing. *Sci. Rep.* **2019**, *9*. [CrossRef] [PubMed]
43. Luo, J.; Jiang, S.; Zhang, H.; Jiang, J.; Liu, X. A novel non-enzymatic glucose sensor based on Cu nanoparticle modified graphene sheets electrode. *Anal. Chim. Acta* **2012**, *709*, 47–53. [CrossRef] [PubMed]
44. Chatterjee, A.K.; Chakraborty, R.; Basu, T. Mechanism of antibacterial activity of copper nanoparticles. *Nanotechnology* **2014**, *25*, 135101. [CrossRef]
45. Reddy, G.R.K.; Hyder, M.; Kumar, P.S. Facile preparation of high-performance copper oxide sensors for electroanalysis of hydrogen peroxide. *Mater. Today Proc.* **2017**, *4*, 12457–12469. [CrossRef]
46. Bhushan, M.; Kumar, Y.; Periyasamy, L.; Viswanath, A.K. Facile synthesis of Fe/Zn oxide nanocomposites and study of their structural, magnetic, thermal, antibacterial and cytotoxic properties. *Mater. Chem. Phys.* **2018**, *209*, 233–248. [CrossRef]
47. Ulaeto, S.B.; Mathew, G.M.; Pancrecious, J.K.; Nair, J.B.; Rajan, T.P.D.; Maiti, K.K.; Pai, B.C. Biogenic Ag nanoparticles from neem extract: Their structural evaluation and antimicrobial effects against pseudomonas nitroreducens and aspergillus unguis (NII 08123). *ACS Biomater. Sci. Eng.* **2020**, *6*, 235–245. [CrossRef] [PubMed]
48. Hu, G.; Liang, G.; Zhang, W.; Jin, W.; Zhang, Y.; Chen, Q.; Cai, Y.; Zhang, W. Silver nanoparticles with low cytotoxicity: Controlled synthesis and surface modification with histidine. *J. Mater. Sci.* **2018**, *53*, 4768–4780. [CrossRef]
49. Kongoli, F.; Marquis, F.; Chikhradze, N.; Prikhna, T. (Eds.) *SIPS2019 Volume 11 New and Advanced Materials, Technologies, and Manufacturing*; FLOGEN Stars Outreach: Mont-Royal, QC, Canada, 2019.
50. Lampé, I.; Beke, D.; Biri, S.; Csarnovics, I.; Csík, A.; Dombrádi, Z.; Hajdu, P.; Hegedűs, V.; Rácz, R.; Varga, I.; et al. Investigation of silver nanoparticles on titanium surface created by ion implantation technology. *Int. J. Nanomed.* **2019**, *14*, 4709–4721. [CrossRef]
51. Juan, L.; Zhimin, Z.; Anchun, M.; Lei, L.; Jingchao, Z. Deposition of silver nanoparticles on titanium surface for antibacterial effect. *Int. J. Nanomed.* **2010**, *5*, 261–267. [CrossRef]
52. Wang, Y.; Gao, Y.; Xu, G.; Liu, H.; Xiang, Y.; Cui, W. Accelerated fabrication of antibacterial and osteoinductive electrospun fibrous scaffolds via electrochemical deposition. *RSC Adv.* **2018**, *8*, 9546–9554. [CrossRef]
53. Lu, X.; Zhang, B.; Wang, Y.; Zhou, X.; Weng, J.; Qu, S.; Feng, B.; Watari, F.; Ding, Y.; Leng, Y. Nano-Ag-loaded hydroxyapatite coatings on titanium surfaces by electrochemical deposition. *J. R. Soc. Interface* **2011**, *8*, 529–539. [CrossRef] [PubMed]
54. Sharma, V.K.; Yngard, R.A.; Lin, Y. Silver nanoparticles: Green synthesis and their antimicrobial activities. *Adv. Colloid Interface Sci.* **2009**, *145*, 83–96. [CrossRef] [PubMed]
55. Niño-Martínez, N.; Martínez-Castañón, G.A.; Aragón-Piña, A.; Martínez-Gutierrez, F.; Martínez-Mendoza, J.R.; Ruiz, F. Characterization of silver nanoparticles synthesized on titanium dioxide fine particles. *Nanotechnology* **2008**, *19*, 65711. [CrossRef] [PubMed]
56. Gaviria, J.; Alcudia, A.; Begines, B.; Beltrán, A.M.; Villarraga, J.; Moriche, R.; Rodríguez-Ortiz, J.A.; Torres, Y. Synthesis and deposition of silver nanoparticles on porous titanium substrates for biomedical applications. *Surf. Coat. Technol.* **2021**, *406*, 126667. [CrossRef]
57. ASTM F67-13(2017). *Standard Specification for Unalloyed Titanium, for Surgical Implant Applications (UNS R50250, UNS R50400, UNS R50550, UNS R50700)*; ASTM International: West Conshohocken, PA, USA, 2017.
58. Torres, Y.; Trueba, P.; Pavón, J.; Montealegre, I.; Rodríguez-Ortiz, J.A. Designing, processing and characterisation of titanium cylinders with graded porosity: An alternative to stress-shielding solutions. *Mater. Des.* **2014**, *63*, 316–324. [CrossRef]
59. ASTM C373-14(2014). *Standard Test Method for Water Absorption, Bulk Density, Apparent Porosity, and Apparent Specific Gravity of Fired Whiteware Products, Ceramic Tiles, and Glass Tiles*; ASTM International: West Conshohocken, PA, USA, 2014.
60. Trueba, P.; Beltrán, A.M.; Bayo, J.M.J.M.; Rodríguez-Ortiz, J.A.; Larios, D.F.; Alonso, E.; Dunand, D.C.; Torres, Y.; Beltran, A.M.; Bayo, J.M.J.M.; et al. Porous titanium cylinders obtained by the freeze-casting technique: Influence of process parameters on porosity and mechanical behavior. *Metals* **2020**, *10*, 188. [CrossRef]
61. Lee, P.C.; Melsel, D. Adsorption and surface-enhanced raman of dyes on silver and gold sols. *J. Phys. Chem.* **1982**, *86*, 3391–3395. [CrossRef]
62. Vlčková, B.; Moskovits, M.; Pavel, I.; Šišková, K.; Sládková, M.; Šlouf, M. Single-molecule surface-enhanced Raman spectroscopy from a molecularly-bridged silver nanoparticle dimer. *Chem. Phys. Lett.* **2008**, *455*, 131–134. [CrossRef]
63. Pavel, I.; McCarney, E.; Elkhaled, A.; Morrill, A.; Plaxco, K.; Moskovits, M. Label-free SERS detection of small proteins modified to act as bifunctional linkers. *J. Phys. Chem. C Nanomater. Interfaces* **2008**, *112*, 4880–4883. [CrossRef]
64. Cuellar-Flores, M.; Acosta-Torres, L.S.; Martínez-Alvarez, O.; Sánchez-Trocino, B.; de la Fuente-Hernández, J.; Garcia-Garduño, R.; Garcia-Contreras, R. Effects of alkaline treatment for fibroblastic adhesion on titanium. *Dent. Res. J.* **2016**, *13*, 473–477. [CrossRef]
65. Wang, Q.; Zhou, P.; Liu, S.; Attarilar, S.; Ma, R.L.W.; Zhong, Y.; Wang, L. Multi-scale surface treatments of titanium implants for rapid osseointegration: A review. *Nanomaterials* **2020**, *10*, 1244. [CrossRef] [PubMed]
66. Tavares, M.G.; de Oliveira, P.T.; Nanci, A.; Hawthorne, A.C.; Rosa, A.L.; Xavier, S.P. Treatment of a commercial, machined surface titanium implant with H2SO4/H2O2 enhances contact osteogenesis. *Clin. Oral Implant. Res.* **2007**, *18*, 452–458. [CrossRef] [PubMed]
67. Takeuchi, M.; Abe, Y.; Yoshida, Y.; Nakayama, Y.; Okazaki, M.; Akagawa, Y. Acid pretreatment of titanium implants. *Biomaterials* **2003**, *24*, 1821–1827. [CrossRef]

68. Bauer, A.W.; Kirby, W.M.M.; Sherris, J.C.; Turck, M. Antibiotic susceptibility testing by a standardized single disk method. *Am. J. Clin. Pathol.* **1966**, *45*, 493–496. [CrossRef] [PubMed]
69. Trueba, P.; Navarro, C.; Rodríguez-Ortiz, J.A.; Beltrán, A.M.; García-García, F.J.; Torres, Y. Fabrication and characterization of superficially modified porous dental implants. *Surf. Coat. Technol.* **2021**, *408*, 126796. [CrossRef]
70. Wu, K.H.; Chang, Y.C.; Tsai, W.Y.; Huang, M.Y.; Yang, C.C. Effect of amine groups on the synthesis and antibacterial performance of Ag nanoparticles dispersed in aminosilanes-modified silicate. *Polym. Degrad. Stab.* **2010**, *95*, 2328–2333. [CrossRef]
71. Frattini, A.; Pellegri, N.; Nicastro, D.; De Sanctis, O. Effect of amine groups in the synthesis of Ag nanoparticles using aminosilanes. *Mater. Chem. Phys.* **2005**, *94*, 148–152. [CrossRef]
72. Pris, M.; Krzysztof, T. Influence of Different Parameters on Wet Synthesis of Silver Nanoparticles. Bachelor's Thesis, University of Twenty, Enschede, The Netherlands, 2008.
73. Drew, W.L.; Barry, A.L.; O'Toole, R.; Sherris, J.C. Reliability of the Kirby-Bauer disc diffusion method for detecting methicillin-resistant strains of Staphylococcus aureus. *Appl. Microbiol.* **1972**, *24*, 240–247. [CrossRef] [PubMed]